Non-linear elastic properties of actin patches to partially rescue yeast endocytosis efficiency in the absence of the cross-linker Sac6

Belbahri Reda, Michelot Alphée, Heuvingh Julien, Du Roure Olivia

Non-linear elastic properties of actin patches to partially rescue yeast endocytosis efficiency in the absence of the cross-linker Sac6.

Belbahri Reda[1,2], Michelot Alphée[2], Heuvingh Julien[1], du Roure Olivia[1]

1, PMMH, CNRS, ESPCI Paris, Université PSL, Sorbonne Université, Université de Paris, Paris, France

2, Aix Marseille Univ, CNRS, IBDM, Turing Centre for Living Systems, Marseille, France

julien.heuvingh@espci.fr, olivia.duroure@espci.fr

Abstract

Clathrin mediated endocytosis is an essential and complex cellular process involving more than 60 proteins. In yeast, successful endocytosis requires counteracting a large turgor pressure. To this end, yeasts assemble actin patches, which accumulate elastic energy during their assembly. We investigated the material properties of reconstituted actin patches from a wild-type (WT) strain and a mutant strain lacking the cross-linker Sac6 (*sac6Δ*), which has reduced endocytosis efficiency in live cells. We hypothesized that a change in the viscous properties of the actin patches, which would dissipate more mechanical energy, could explain this reduced efficiency. There was however no significant difference in the viscosity of both types of patches. However, we discovered a significantly different non-linear elastic response. While WT patches had a constant elastic modulus at different stresses, *sac6Δ* patches had a lower elastic modulus at low stresses, before stiffening at higher ones, up to values similar to WT patches. To understand the consequences of this discovery, we performed, *in-vivo,* a precise analysis of actin patch dynamics. Our analysis reveals that a small fraction of actin patches successfully complete endocytosis in *sac6Δ* cells, provided that those assemble an excess of actin at the membrane compared to WT. This observation indicates that non-linear elastic properties of actin networks in *sac6Δ* cells contribute to rescue endocytosis, requiring nevertheless more actin material to build-up the necessary stored elastic energy.

Introduction

Non-linear mechanical response is a well-known occurrence of biological materials and specifically of cytoskeleton[1]. Stress-stiffening behavior has been intensively observed and studied in dilute solutions of actin filaments, entangled or crosslinked by proteins or molecular motors. This mechanical behavior has been identified to originate from an entropic effect associated to the reduced number of accessible entropic configurations for the actin filaments inside the meshwork[2]. It is still present but less pronounced in presence of crosslinkers[3,4]. Denser actin gels, despite their importance in many cellular functions, have been characterized less thoroughly for their mechanical properties. Such gels are more difficult to investigate as they require the local assembly and concentration of micrometer-scale networks. A typical example is that of dendritic actin networks, where short actin filaments are nucleated and branched by the Arp2/3 complex, and capped by capping protein[5–7]. A few studies have nevertheless reported mechanical measurements showing a nonlinear behavior[8–10] which is more difficult to attribute to entropic effects as the typical filament length is much shorter than in the dilute case. Actin gels that are assembled with the minimal required number of proteins and under higher

forces are stiffer and still respond nonlinearly to stress independently of the presence of crosslinking proteins[9]. The effect of crosslinkers on non-linear mechanics in actin gels assembled from the whole set of actin binding proteins present in the cytoplasm, has not yet been studied. Dendritic actin networks play a major role in different physiological processes, such as endocytosis in the context of which we placed our contribution to this special issue.

Endocytosis is the formation and internalization of a vesicle at the outer membrane of an eukaryotic cell[11,12]. These vesicles – of approximately 100 nm size - transport molecular cargos from the exterior of the cell to its interior and contribute to plasma membrane recycling and homeostasis. Typical uptake cargoes include nutrients, neurotransmitters, pheromones or signaling molecules. Several cellular machineries involved in endocytosis have been described, one of them being Clathrin-Mediated Endocytosis (CME)[13]. The curving of the initially and spontaneously flat plasma membrane into a sphere of a small diameter has an energetic cost that needs to be compensated[14]. In CME, clathrin proteins assemble onto the membrane into a scaffold (or cage) that has a positive spontaneous curvature. The energy brought by this assembly can be sufficient to form spherical vesicles of appropriate diameter on floppy membranes. However, tension in the plasma membrane adds an energetic cost as the surface of the membrane needs to expand during the formation of a vesicle. Additionally, the entropic fluctuations of proteins attached to the membrane outside and inside the vesicle respectively reduce and increase this energetic cost[14]. Finally, the polymerization of actin filaments, which is essential for the migration of eukaryotic cell, plays also an important role in the energetic balance of membrane invagination. In mammalian cells, actin polymerization is required for successful endocytosis on cells with a high membrane tension, but not when membrane tension is reduced[15]. In yeast cells, where turgor pressure has an additional opposing force that overshadows all the previously described ones, actin polymerization is essential for successful internalization[16–18] . The magnitude of this pressure has been estimated at 1 MPa, and cells are only able to withstand this pressure because of the existence of a rigid and permeable cell wall [17,19–22]. The dominant hypothesis is that actin polymerization provides the main force required to overcome turgor pressure in yeast[18,23–25].

Endocytic actin networks assemble as patches, about 15 seconds before the end of a 2 min complex sequence of events where numerous protein partners are progressively recruited at the yeast membrane[26]. These patches can be easily observed by microscopy as yeast lacks an actin cortex that would obscure similar patches in animal cells. Yeast is therefore an excellent model system to understand actin-based force generation during endocytosis. As quantitative observations of individual molecules recruited during yeast endocytosis became more common, an inconsistency appeared: although 100-150 filaments are present in the few-hundred-nm-wide patch of actin that are pushing the vesicle inward[26], only a part - from 8 [27] to 100 [28] - are actively pushing at a given time due the finite nucleation rate and the capping events. As each filament develops a maximal force between 1 and 10 pN [29], their assembly should generate a force of 10-1000 pN to overcome a force of approximately 3000 pN induced by the turgor pressure[30]. This order of magnitude discrepancy has garnered a large number of hypotheses[29,31]. The osmotic pressure could be locally relaxed[31], the angle of the filaments to the membrane could be such that a lever effect could be harnessed to increase the mechanical work of this force[23], finally myosin motors could play a role, to help insert new monomers at the polymerizing tip of actin filaments in contact with the membrane[32].

Another elegant solution to this problem lies into the storage of elastic energy in actin networks during its assembly, through crosslinkers[33] or filaments themselves[25]: if most of the energy produced by actin filament polymerization is invested in the deformation of filaments inside the network, energy from many filaments can be cumulated through the patch assembly until large enough to overcome the turgor pressure; it can then be released to induce the formation and internalization of the vesicle. At the onset of endocytosis, the surface of the endocytic patch is circular, and stronger forces are exerted on the outer region than on the central region. The actin network is attached to the central region through actin-binding clathrin adaptors like Sla2 or Ent1 [12]. The polymerization of actin occurs preferentially in the outer region where the activator of Arp2/3 (Las17, analog of WASp in yeast) is present. At the beginning, the polymerization is not constrained and the network assembles without feeling external forces. However, as the central region is anchored to the membrane, the polymerizing actin network feels the turgor pressure applied to the membrane while it grows in size is limited. As a result the patch deforms and the force generation problem shifts from force production by individual filaments to viscoelastic properties of the actin patch itself: the energy will be stored in the elastic deformation of the patch while it will be dissipated by its viscous response. Such mechanism is also at the core of theoretical studies of force-generation during endocytosis using either an active gel approach[34] or continuous mechanics models[18]. The non-linearity of the mechanical properties, such as the stress-stiffening observed on *in vitro* dendritic actin networks[9,10] should also affect crucially the energy stored in the elastic deformation, as a soft initial regime when the actin network is slightly deformed would hamper the accumulation of stored elastic energy. Crucial to efficient plasma membrane invagination in yeast CME is the presence of the protein Sac6p[16,35–37], a homolog of mammalian fimbrin, which bundles and crosslinks the filaments together[38]. Due to its role as a key element of actin architecture, Sac6p is expected to have a strong effect on the mechanical response of actin networks[39].

We thus decided to investigate the material properties of actin reconstructed from yeast extracts. In these experiments, grafting of a nucleation promoting factor of the Arp2/3 complex at the surface of a particle is sufficient to reconstitute the assembly of actin structures similar to those present in the cell[40]. In particular, these reconstituted patches contain the numerous actin associated proteins present at endocytic sites in vivo. We focused on comparing patches assembled from wild-type (WT) and mutant strains lacking Sac6p (*sac6Δ*) due to their difference in endocytosis efficiency in vivo. We have previously shown than Sac6p was the only actin crosslinker with an effect on the elasticity of actin patches in yeast[37]. Our previous study used magnetic beads as a support of the gel and as indenters, which are devices of choice to measure a large number of samples[41]. However the spherical zone of contact precludes thorough studies of the viscosity and non-linear behavior. We thus chose to use magnetic cylinders that deform the gels between two flat surfaces[10]. Our approach allows the study of the endocytic events in vivo, as well as the material properties of actin patches in vitro, from the same strains.

Experimental

Yeast cell imaging and analysis

Yeast strains were grown at 25°C up to 0.5 < Optical Density (OD) < 0.7. For observation under the microscope, cells were immobilized on coverslips coated concanavalin A (0.1 mg/mL). Live cell imaging was achieved on a Zeiss Axio Observer Z1 microscope using a 100×/1.4 NA oil Ph3 Plan-Apochromat

objective (Zeiss, Oberkochen, Germany) and a Hamamatsu ORCA-Flash 4.0 LT camera (Hamamatsu, Hamamatsu City, Japan). Zen 2.3 blue edition software was used to control the microscope.

The dynamic of endocytic actin patches was tracked using the Fiji plugin TrackMate[42], as described previously[37]. Individual patches were isolated from the rest of the cell using a median filter and a difference of Gaussian (DoG) particle detection algorithm for areas with a diameter of approximately 0.5 µm and a contrast above 0.1. To be considered as an actual patch, the lifetime should be larger than 5 seconds and the intensity should first increase and then decrease. We only considered patches for which the full dynamics is included in the movie. Patch lifetime, which was defined as the time during which the intensity of the patch is larger than the threshold, and the maximum intensity were extracted for each patch and processed through custom scripts in MATLAB R2020b (The Math-Works, Natick, MA, USA). The intensity has been corrected for photobleaching effects, which were estimated by fitting a linear curve to the temporal evolution of the whole cell intensity.
A successful endocytic event is defined as an event for which the internalization has undergone displacement larger than 200 nm which is a typical choice in the literature[43].

Yeast extract preparation

Yeast extracts was prepared following Michelot et al[44]. Yeast strains were cultured in standard rich medium (YPD) at 30 °C to an OD_{600} of 1.5-2, harvested by two successive centrifugations. Liquid N_2 was used to flash freeze pellets and pellets were grounded by mechanical shearing in a Waring blender. To prepare an experiment, one gram of yeast powder was rehydrated in $100\ \mu L$ of HEPES buffer (100 mM, pH 7.5) in presence of 10 μL of protease inhibitors (Cocktail Set IV, Calbiochem, Merck4Biosciences). We first gently mixed on ice, progressively thawed, and centrifuged for 20 minutes at 50,000 x g. We collected the clear supernatant, kept it on ice, and used it within 3 hours.

Cylinder fabrication and functionalization

Magnetic cylinders were fabricated according to (Tavacoli 2013). Briefly, an array of wells were fabricated in polydimethylsiloxane (PDMS) using soft lithography. The molds were filled with a mixture of monomeric ethoxylated trimethylolpropanetriacrylate (ETPTA), thermo-initiator, and 50% w/w superparamagnetic small colloids, before being cured at 130 °C for 2 hours.

A band (2 cm x 1-2 mm x 1 mm) of the PDMS mold was cut and cleaned with plasma, silanised with chlorotrimethylsilane for 30 min. The band is functionalized by putting it in a HEPES solution containing 2.5 $\mu g/L$ of BSA-Biotin. These treatments allow a functionalization of the top surface of the cylinder with BSA-biotin. The band is then bent into a small tube containing a 1% solution of bovine serum albumin (BSA) and sonicated for 10-30 min to help the extraction. The surfaces that were previously protected by the mold can now be covered by BSA. We obtain then a unique surface covered with BSA-biotin while the rest of the surfaces are passivated with BSA. The cylinders are then incubated with 1 $\mu mol/L$ Streptavidin-Las17(375-Cter)-6xHis which will bind to biotin. Magnetic cylinders functionalized with Las17 were used on the same day.

Experimental setup for mechanical characterization

The experimental setup for the observation and magnetic field application consists of a Zeiss Axio A1 inverted microscope with a 100x/1.4 NA oil immersion Apochromat and a modified stage hosting two

coils with a soft iron core generating a constant magnetic field in the chamber between 0 and 80 mT. A bipolar operational power supply (Kepco, New York City, NY, USA) feeds the coil with up to 5 A electrical current corresponding to an 80 mT homogenous magnetic field in the chamber. A Labview (National Instruments, Austin, TX, USA) custom program controls the field and the image acquisition. Timelapses are recorded with an ORCA Flash 4.0 CMOS camera (Hamamatsu). 1 μL of functionalized cylinders are mixed with 9 μL of yeast extract. The mixture is introduced into a homemade flow chambers. Chambers are sealed with a mix of 1/3 Vaseline, 1/3 Lanolin, and 1/3 paraffin.

Force and distance analysis

The evolution of the gel length l between two cylinders is calculated from the sub-pixel correlation of two regions of interest drawn inside each cylinder[10]. For each ROIs, the estimate error on the displacement is around 2.5 nm. The correlation of the displacements of the ROIs gives a relative and precise modification of the gel length. The gel length on the first image l_0 of the video is measured on the profile plot of the pair of cylinders using a script (*findchangepts* in Matlab) finding abrupt changes in the contrast. A calibration with small (1µm) magnetic beads allowed for a correction from the apparent optical length to the actual physical length and led to error estimation on the initial thickness of 63 nm, improved from[10].

The force F applied by two cylinders is calculated as described previously[10], using finite element analysis, and taking into account the cylinder lengths, distances and magnetic susceptibility as well as the applied magnetic field. The mechanical stress is calculated by simply dividing the force by the surface S of the cylinder face (π x 3^2 µm^2), that was prescribed by the mold shape.

Data analysis for step compressions

For reconstituted patches growing between two cylinders, we can define a stress $\sigma = F/S$ and a strain $\epsilon = \frac{l-l_0}{l_0}$, where l_0 is the initial length, F the force between the cylinders and S the surface of the cylinder face (a 6 µm diameter disk). The actin patch was deformed with a 60 sec-compression step. The value of the plateau σ_0 depends on the length of the patch and has a mean of 64 +- 28 Pa.

Response to step compression was analyzed using Burger's viscoelastic model. This model consists of a series of: a Maxwell module made of a spring with an elastic modulus $E_{instantaneous}$, in series with a dashpot of viscosity $\eta_{irreversible}$ and a Kelvin Voigt module itself composed of a spring of elasticity E_{KV}, and a dashpot of viscosity η_{KV} in parallel (see figure 1B insert).

The Burger's model gives an evolution for the strain ϵ for step of compression from $\sigma = 0$ to σ_0 :

$$\epsilon(t) = -\sigma_0 \left(\frac{1}{E_{instantaneous}} + \frac{1}{E_{kv}} \right) - \frac{\sigma_0}{\eta_{irreversible}} \cdot t - \frac{\sigma_0}{E_{kv}} \left(1 - e^{-\frac{t}{\tau_{kv}}} \right)$$

where t_{KV}=η_{KV} / E_{KV}

This can be written as:

$$l(t) = p_2 + p_1 \cdot t + a_0 \cdot e^{-\frac{t}{\tau_{kv}}}$$

We used this expression to fit experimental data and divided the fit into two parts:

-Fit the linear part (curve (3) in fig 1B) for t>30 s, where $l(t) = p_2 + p_1 \cdot t$ then,

$$\eta_{irreversible} = -\frac{\sigma_0\, l_0}{p_1}$$

-With the calculated parameters, we fit the exponential part (curve (2) in fig 1B), to obtain a_0 and τ_{kv}

$$E_{kv} = \frac{\sigma_0\, l_0}{a_0}$$

$$\eta_{kv} = E_{kv} \cdot \tau_{kv}$$

We calculate the instantaneous deformation $l_{inst} = l_0 - p_2 - a_0$ (curve (1) in fig 1B) which gives

$$E_{instantaneous} = \frac{\sigma_0\, l_0}{l_0 - l_{inst}}$$

We also define an equivalent elasticity $E_{total} = \frac{1}{\frac{1}{E_{kv}} + \frac{1}{E_{instantaneous}}}$

Non-linear elasticity

Probing the non-linearity has been done by increasing the magnetic field from the minimal value to hold the cylinders in contact, up to the maximum value possible in our setup in the course of 1 to 7 seconds. Because the force between the cylinders varies with their distance to one another, the extreme values of the applied stress are not the same for each actin gel tested. The gel thickness evolution during the compression gives the stress-strain curve. The non-linear elasticity is measured using the tangent modulus $K = -\frac{d\sigma}{d\epsilon}$. The tangent modulus is the slope of the tangent of the stress-strain curve. For the tangent fit, we discretize the stress into "targets". For each target, we take the neighboring points and weigh them with a gaussian, where the maximum is the target and as we get further away from the target the weight decreases. Using this, we fit the tangent to get the slope, thus the tangent modulus, for targets: 10 Pa and 50 Pa. As the loading time is markedly lower than the characteristic time of the Kelvin Voigt part of the model measured with step force, the Kelvin Voigt part is expected to behave as a dashpot. We corrected the measured strain by integrating the stress felt by the network since the start of the compression and using the medium viscous value obtained previously.

Statistical analysis

To compare results of the fits on multiple actin patches, we pool the results and compare them between conditions using a Wilcoxon-Mann-Whitney analysis. Exact p-values inferior to 10^{-3} were reported as $p < 10^{-3}$. The number of analyzed compressions for the visco-elastic analysis was 71 / 28 in 18 / 9 independent reconstituted patches for WT / sac6Δ. Non-linear elasticity was analyzed in 11 / 12 independent reconstituted patches for WT / sac6Δ. Lifetime and intensity of *in vivo* patches was analyzed on 121 /99 patches on 16 /23 different cells for WT/ sac6Δ.

Materials

Standard procedures were used to generate yeast mutants as described in Longtime *et al.*[45].Two mutant lines, derived from S228C strain, were used: Abp1-GFP and Abp1-GFP *sac6Δ*.

The nucleation promoting factor of the Arp2/3 complex used in this study is based on a truncation of *S. cerevisiae*'s Las17p (Gst-TEV-Streptavidin-Las17(375-Cter)-6xHis), which is the yeast homologue of

WASp. The protein was expressed and purified from *Escherichia coli* Rosetta 2(DE3)pLysS cells as described in Antkowiak *et al* [46].

Silica superparamagnetic colloids of 300 nm in diameter were purchased from Ademtech (France).

Other chemicals include: Protease Inhibitor Cocktail Set IV (Calbiochem, Merck4Biosciences), thermo-initiator Azobisisobutyronitile (AIBN, Sigma), chlorotrimethylsilane (Sigma),BSA-biotin (Sigma), bovine serum albumin (Sigma)

Results

Magnetic cylinders of 6 µm-diameter functionalized on one of their faces with Strep-Las17- protein were incubated with yeast cell extract. The mix of micro-cylinders and extract was introduced into a flow chamber and placed on a microscope equipped with magnetic coils. Experiments were initiated at low (3mT) homogenous magnetic field. The cylinders aligned their long axis along the field lines due to the magnetic torque[47] and formed chains of 2 to 5 cylinders due to their dipolar magnetic attraction. Reconstituted actin patches grew from the functionalized face at a speed of approximately 0.2 µm/min, before levelling off. Actin gels were observed through fluorescence, and were also visible in phase contrast between two cylinders as faint structures that prevent two neighbouring cylinders from contacting each other (Figure 1A). For each experiment, a chain of cylinders with one or several actin gels grown between functionalized and passivated faces was selected from the numerous chains formed in the experimental chamber. When the magnetic field was increased (up to 80 mT), the force between the cylinders was increased as well (up to a few nN) inducing deformation of the actin network. This deformation was monitored by the change in distance between the magnetic cylinders and can be measured at a few nm precision[10].

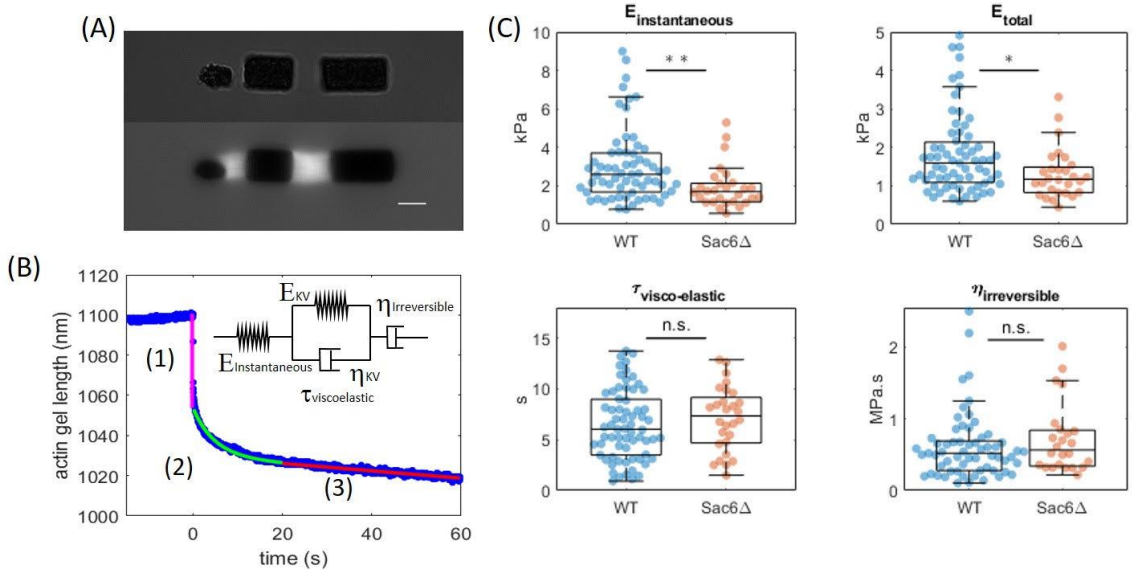

Figure 1. A: bright field (top) and fluorescence (bottom) microscopy image of a pair of magnetic cylinders with reconstituted actin patches grown from one of their face. Only the one on the right was analyzed the one on the left being in contact with a debris. The scale bar is 5 µm. B: typical response of

the length of the gel when submitted to a step increase of stress (here the stress goes from 1.6 to 115 Pa), and associated analysis with (1) instantaneous deformation (2) visco-elastic deformation and (3) irreversible viscous flow. Inset: Burger's *model used for the analysis (see text for details). C: Comparison of the actin network's material properties grown from the cell extracts of WT yeast and mutants lacking Sac6p crosslinker.*

To investigate the viscoelastic properties of the actin network, we imposed a series of step compressions on the actin network from low to high stresses. Upon compression (figure 1B), the length of the actin network instantaneously decreased (phase 1 in figure 1B). After a curved transition (phase (2)), the length continued to decrease linearly but at a much slower rate (phase 3 in figure 1B). This behavior is reminiscent of Burger's viscoelastic model commonly used to model the mechanical response of cells[48,49]. This model consists of a spring with an elastic modulus $E_{instantaneous}$, a dashpot of viscosity $\eta_{irreversible}$ and a Kelvin Voigt (KV) module (composed of a spring, E_{KV}, and a dashpot, η_{KV}, in parallel) in series (figure 1B insert). The spring accounts for the instantaneous deformation (phase 1 in figure 1B) the dashpot for the long-time yield (phase 3) and the Kelvin Voigt module for the transition between the two other regimes (phase 2). We fitted these four physical parameters (figure 1C, see experimental section for details on the fitting procedure). For wild-type patches, the obtained elastic instantaneous modulus ($E_{instantaneous}$) had a median of 2.7 kPa (quartile: 1.8 to 3.9 kPa). The viscosity at longer time which creates an irreversible deformation ($\eta_{irreversible}$) had a median of 490 kPa.s (260 to 680 kPa.S). From the parameters of the Kelvin Voigt module, we obtained a viscoelastic time scale $\tau_{visco-elastic}$ of 6.0 s (3.5 to 9.0 s), and we can calculate the total elasticity E_{total} (a combination of both types of elasticity) of the system of 0.63 kPa (0.47 to 0.92 kPa).

The observation of an irreversible viscous part in the mechanical properties of the yeast actin network is crucial in the framework of force generation in endocytosis as it will dissipate part of the energy furnished by the elongation of actin filaments and limit the energy useful to internalize the vesicle. We thus reproduced the mechanical characterization with *sac6Δ* extracts. The absence of the actin crosslinker Sac6p, which partially inhibits yeast endocytosis, is expected to change the viscoelastic properties of the reconstructed network. In *sac6Δ* extracts, dense actin networks grew similarly from the functionalized face of the cylinder, but at an elevated speed of 0.4 µm/min compared to wild-type extracts. They were subjected to the same stress cycles and analyzed similarly using the Burger's model. We obtained from these gels a lower $E_{instantaneous}$ of median 1.7 kPa (1.2 to 2.1 kPa). Comparison of the instantaneous elasticity yield a significant difference between WT and *sac6Δ* ($p< 10^{-3}$). On the contrary, neither the viscosity $\eta_{irreversible}$ nor $\tau_{visco\text{-}elastic}$ yielded significant differences – median of respectively 517 kPa.s (p=0.44) and 7.35 s (p =0.33) - infirming the hypothesis that a network lacking Sac6p would yield more under the stress developed during actin patch growth and thus reduce the efficiency of endocytosis.

As the instantaneous modulus was the main signal of difference between WT and *sac6Δ* reconstituted networks, we conducted experiments to characterize more thoroughly this property, and in particular its non-linear behavior as function of stress. We thus deformed progressively WT and *sac6Δ* actin patches by increasing the magnetic field from 2mT to 60mT, resulting in an increase of the stress from a fraction of Pascal to a few tens of Pascal, the exact value depending on the length of the network (see Experimental section). Typical deformation as a function of the stress is presented in fig 2A, and show a markedly different behavior between networks prepared from WT and *sac6Δ* extracts. While WT networks exhibited a linear compression with the stress, the networks grown from *sac6Δ* extracts

exhibited a stress-stiffening response. The absence of the Sac6 crosslinker thus induced a non-linear elastic response in the branched network. To quantify this effect, we measured the slope of the strain-stress curves for different stresses (in the previous experiment, as the deformation was instantaneous, no such analysis could be done). While the tangent elastic modulus (K) is rather constant for the WT network (around 700 Pa for the gel shown on fig 2A), it increased steadily from 300 at low stress to 1500 Pa at 80 Pa stress for networks grown from *sac6Δ* extracts. We reported the values of K at 10 Pa and 50 Pa stress for all grown networks in fig 2B. While the mutant networks are significantly softer than the WT at a stress of 10 Pa ($p = 2.5\ 10^{-2}$), they have similar moduli at a stress of 50 Pa ($p = 0.31$). Defining the ratio of the moduli at 50 Pa to the one at 10 Pa – Non Linear Index- as a measure of the material's non-linearity, we obtained a median ratio of 1.3 for WT, and 2.4 for *sac6Δ.* These results show that the WT reconstituted patches are mostly linear in their elasticity, while the patches lacking the sac6 crosslinker exhibit a significantly more important stress-stiffening behavior ($p = 8\ 10^{-3}$).

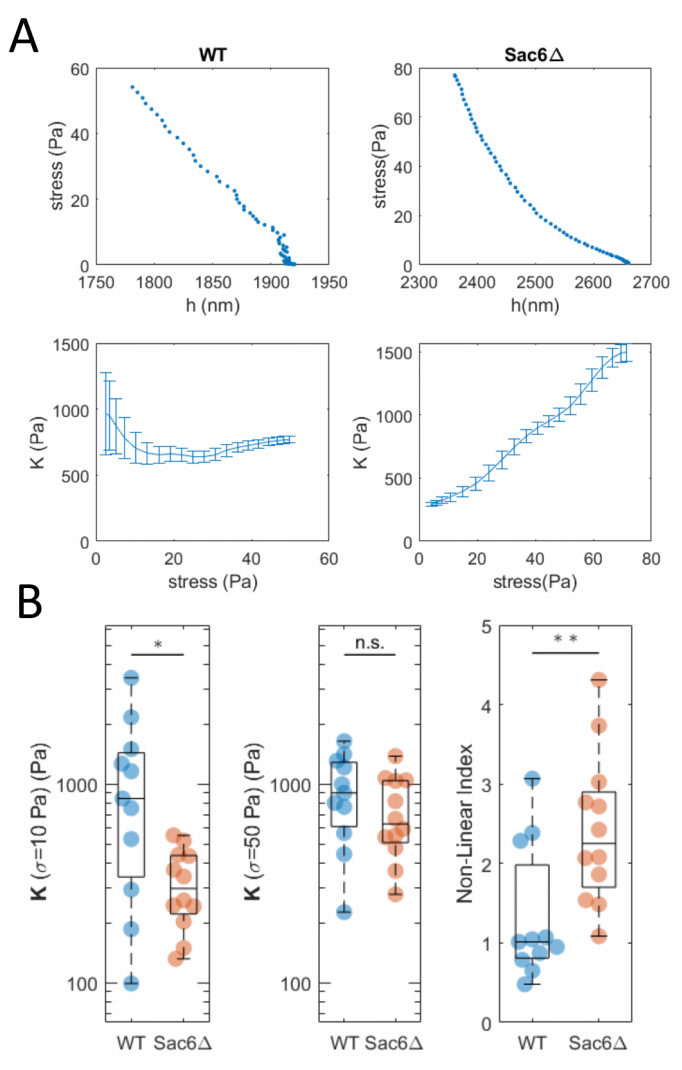

Figure 2. A: Typical deformation of actin networks (WT and sac6Δ) during a ramp of stress, and associated tangent elastic moduli as function of stress. B: tangent elastic moduli at 10 and 50 Pa stresses as well as their ratio (Non Linear Index).

This stark change in the linearity of the gel mechanical response when its principal crosslinker is absent is expected to have a strong effect on the network's ability to generate forces. At low stress, the low

elastic modulus of *sac6Δ* actin patches would result in a large deformation with a lower rate of elastic storage. At higher stresses, the network elastic characteristic would be more comparable to WT strains and eventually develop similar elastic stresses. This would result in a *successful* internalization at the cost of a longer and more important accumulation of actin material.

To test this hypothesis in live cells, we followed endocytosis in the same strains as the ones used to prepare cell extracts whose mechanics has been characterized in figure 1 and 2 (see Experimental section and Planade *et al*[37]). Yeast cells lacking Sac6p are known to have a larger number of actin patches and a large part of them fail to internalize a vesicle[16,35–37]. We here considered, for both strains, only the endocytic events that have been successful and that are defined as the ones internalizing more than 200 nm from the plasma membrane. Figure 3 compares the dynamics of such successful patches in the two strains. Figure 3A shows typical temporal evolution of the fluorescence intensity for two representative patches in each strain. Initial time points were defined as the instants when actin networks begin to visibly grow. The general trend observable here is that successful endocytic events are faster and require less assembled actin in WT strains as compared to *sac6Δ* strains. This observation is confirmed by quantitative measurements of patch lifetime (figure 3B) and maximal patch intensity (figure 3C). In strain lacking Sac6p, successful endocytic patch lifetime median is 66% longer than in wild type strain (10 sec vs 6 sec, $p<10^{-3}$) and accordingly successful patches have 28% more actin material (median of the maximal intensity in *sac6Δ*, 0.0176 a.u. vs in WT, 0.0137 a.u., $p< 10^{-3}$).

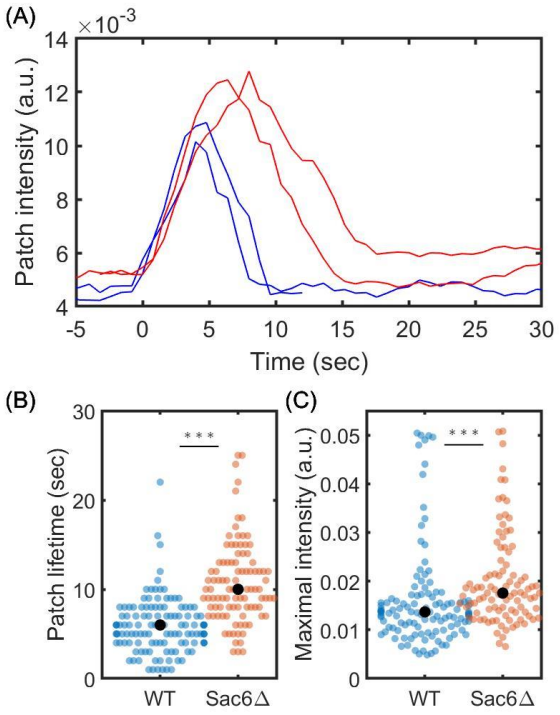

Figure 3: Measurements of successful endocytic patch dynamics in yeast cells. (Top) Typical temporal evolution of the fluorescence intensity of two patches as a function of time for WT (blue) strain and sac6Δ (red) mutant. The patch intensity is calculated as the ratio of the fluorescence intensity normalized by the overall intensity of the cell. (B) Patch lifetime (left) and maximal intensity (right) for the two strains. Black dots correspond to the median of each distribution.

Discussion

In the study reported here we precisely quantified the viscoelastic behavior as well as the nonlinear properties of reconstituted actin patches assembled from WT and a mutant lacking the protein Sac6p. The viscoelasticity is analyzed in the framework of the Burger's model which combines to elementary viscoelastic modules each built by a combination of a spring and a dashpot either in series – Maxwell module – or in parallel – Kelvin Voigt module. A spring allows for elastic energy storage while a dashpot dissipates energy irreversibly. When combined in a viscoelastic module, depending on their relative arrangement, the global behavior – storage or dissipation - depends on the timescale considered and one can build a characteristic timescale – η/E – that separates the dissipation-dominated region and the storage-dominated region. To store elastic energy, a Maxwell module is efficient at short timescale as the spring responds quicker than the dashpot but at long time scale all the energy initially stored in the spring is dissipated by the dashpot. We found 154 s for the Maxwell timescale for WT reconstituted patches and 358 s for *sac6Δ* reconstituted patches, values that are far larger than the typical lifetime of the patches in vivo. Thus, for both strains the Maxwell viscosity does not play any role and does not dissipate the energy during the patch assembly. The Kelvin-Voigt module, on its side, works in the opposite way to the Maxwell module: the elastic storage is slowed down by the presence of the dashpot in parallel and will be maximum after the typical characteristic time η/E which is for both strains around 6 sec. This value is on the same order of magnitude of the patch lifetime (6 sec for WT strain, and 10 sec for *sac6Δ* strain) but small enough so that the energy generated by the elongation of the actin filaments in the patch is mainly stored in elastic deformations. In conclusion, the two strains have similar behavior in terms of viscoelasticity and the difference observed here cannot explain the failed endocytosis phenotype in mutant lacking Sac6p. We then focused on the nonlinear behavior of actin patches.

In endocytic patches, actin is assembled through the Arp2/3 machinery that results in dendritic architecture of the network in which each branch connects three strands only. These networks have thus a lower connectivity than networks with classical crosslinks where each point of contact connects four strands. The architecture and the connectivity have a profound impact on the mechanics of fiber materials[50]. Below a certain percolation threshold, the network cannot stand against deformation, while around the transition, the elasticity increases dramatically. A purely branched network with low number of entanglements points will thus barely resist a force. However, with increasing deformation, more and more contacts between adjacent strands are established leading to stiffer and stiffer response. In terms of mechanics, such networks will thus exhibit a nonlinear elastic behavior characterized by a stress stiffening[10]. Experimentally, actin branched networks reconstituted from purified proteins without crosslinkers, have been shown to have non-linear behavior that depends strongly on the stress the network endured during growth. In a previous study using magnetic cylinders that allow for minimal stress during growth (<1 Pa) we have found a strong stress-stiffening behavior, with a linear dependence between the tangent elastic modulus and the applied stress[10]. The Non Linear Index calculated between 10 and 50 Pa would be of a value of ~5 (to be compared to Non Linear Index of 1-3 measured here). On the contrary, for actin networks grown at 25 Pa (under the tip of an Atomic Force Microscope), no stress stiffening has been observed and Non Linear Index would be close

to 1 [9]. As the application of a stress during growth is expected to increase the number of contacts between actin filaments, this result can be understood as the signature of a change in the initial connectivity of the network. At higher values of growth stress (above 100 Pa), non-monotonic nonlinear behavior appears with an important role of the growth stress[9].

The actin networks in endocytic patches possess in addition classical crosslinkers with 4 connections, and therefore their connectivity is increased as compared to purely branched actin networks, and one can expect that the rigidification induced by the increased number of contacts during deformation will have less impact[9]. This would adequately explain the stark difference we observed between patches reconstituted from WT extract which have a linear elastic behavior, and patches reconstituted from extracts lacking Sac6p, which stiffen with stress. Nonlinear elasticity in branched actin networks reconstituted from Xenopus cell extracts was studied by Chaudhuri et al [8]. They reported a constant elastic modulus at low stresses, a stress-stiffening up to 250 Pa and then a stress softening. We did not observe similar behavior but the biological systems are markedly different. Note also that we explore a smaller range of stress with our setup.

An interesting note is that the values reported here where the reconstituted patches grow from a flat surface (the face of a cylinder) are less important than the ones we previously reported in Planade et al[37], on actin networks growing from the surface of a bead (5.7 and 3.3 kPa for WT and *sac6Δ*) despite the fact that similar cell extracts have been used in the two studies. In a spherical geometry, the recent and growing gel is compressed by the presence of the previous gel on the outer edge of the network. Thus, an internal stress - that can reach kPa values[51,52] develops during the growth. As already mentioned, growth under stress is known to drastically increase the density and stiffness of Arp2/3 actin networks *in vitro* for reconstituted proteins[9] and also *in vivo* in lamelipodia as recently reported[53]. We therefore checked if our reconstituted actin patches also exhibit this behavior. Patches assembled under a field of 40 mT (80 Pa stress) were strongly stiffer (see Supplementary figure) than patches assembled at low stresses confirming the interpretation of the discrepancy between our two measurements. In endocytosis, actin in the patch is subjected to more and more stress as it grows, similarly to the growth around bead. The growth on flat surfaces is however the only way to perform precise measurement by controlling and monitoring the stress the gel is subjected to.

Conclusion

In conclusion, we would like to interpret our results on the mechanics of actin patches in the context of force generation in endocytosis. We recall that due to the large turgor pressure in yeast, the energy produced by the elongation of actin filaments needs to be stored in elastic deformations until large enough. When enough energy has been stored to compensate the mechanical work of the turgor pressure necessary to form the vesicle, the process is almost instantaneous, and the internalization takes place. Here, we investigated the material properties of reconstituted actin patches from a WT strain and a partially defective strain lacking the cross-linker Sac6p. We hypothesized that a change in the viscous properties of the actin patches, which would dissipate more mechanical energy, could explain this reduced efficiency. The viscosity of the patches was however limited and showed no significant reduction when Sac6p was absent. We next discovered that the two types of patches had a significantly different non-linear elastic response. While the normal patches had a constant modulus at different stresses, the patches lacking cross-linkers had a lower elastic modulus at low stresses,

before stiffening up to values similar to the ones of the normal patches. Therefore, the stored elastic energy will be low in the first phase of deformation for patches lacking cross-linkers, but the stored energy can then be accumulated at larger deformation, potentially reaching the necessary threshold for successful endocytosis. This mechanism of rescue by non-linear elastic properties would however require more actin to be assembled in the patch and thus higher assembly time. We verified by analyzing in vivo yeast patches, that in the strain lacking cross-linkers, the subset of successful patches indeed lasted for a longer time and gathered more materials than successful patches in WT strain. The increased duration of the patch lifetime has important biological consequences, as actin is constantly recycled in the yeast cell, and patches accumulating actin for too long would be disassembled by the biochemical machinery of the cell before enough energy has been cumulated, hence failing to produce endocytosis. The patch disassembly has been observed in fission yeast to occur 9-15 sec from the beginning of the assembly[26], right after the average patch lifetime in WT strain (6 sec) but comparable to the average patch lifetime of the mutant strain (10 sec). Actin, Arp2/3 and capping proteins disappear from the patch concomitantly despite their different kinetics showing that the disassembly is associated to severing of the actin filaments, the rapid diffusion of small fragments and their depolymerization. This process is orchestrated by different disassembly factors (like cofilin, Aip1, and coronin)[54–56]. In addition to this local biochemical regulation, at the scale of the cell if too many patches are assembling concomitantly the pool of G-actin may not be large enough and actin depolymerization may become dominant.

Acknowledgments

This project has received funding from the European Research Council (ERC) under the European Union's Horizon 2020 research and innovation program (grant agreement n° 638376/ Segregactin)

(1) Storm, C.; Pastore, J. J.; MacKintosh, F. C.; Lubensky, T. C.; Janmey, P. A. Nonlinear Elasticity in Biological Gels. *Nature* **2005**, *435* (7039), 191–194. https://doi.org/10.1038/nature03521.

(2) Gardel, M. L. Elastic Behavior of Cross-Linked and Bundled Actin Networks. *Science* **2004**, *304* (5675), 1301–1305. https://doi.org/10.1126/science.1095087.

(3) Lieleg, O.; Claessens, M. M. A. E.; Heussinger, C.; Frey, E.; Bausch, A. R. Mechanics of Bundled Semiflexible Polymer Networks. *Phys. Rev. Lett.* **2007**, *99* (8), 088102. https://doi.org/10.1103/PhysRevLett.99.088102.

(4) Schmoller, K. M.; Lieleg, O.; Bausch, A. R. Cross-Linking Molecules Modify Composite Actin Networks Independently. *Phys. Rev. Lett.* **2008**, *101* (11), 118102. https://doi.org/10.1103/PhysRevLett.101.118102.

(5) Cameron, L. A.; Footer, M. J.; van Oudenaarden, A.; Theriot, J. A. Motility of ActA Protein-Coated Microspheres Driven by Actin Polymerization. *Proc. Natl. Acad. Sci.* **1999**, *96* (9), 4908–4913. https://doi.org/10.1073/pnas.96.9.4908.

(6) Pantaloni, D. Mechanism of Actin-Based Motility. *Science* **2001**, *292* (5521), 1502–1506. https://doi.org/10.1126/science.1059975.

(7) Bernheim-Groswasser, A.; Wiesner, S.; Golsteyn, R. M.; Carlier, M.-F.; Sykes, C. The Dynamics of Actin-Based Motility Depend on Surface Parameters. *Nature* **2002**, *417* (6886), 308–311. https://doi.org/10.1038/417308a.

(8) Chaudhuri, O.; Parekh, S. H.; Fletcher, D. A. Reversible Stress Softening of Actin Networks. *Nature* **2007**, *445* (7125), 295–298. https://doi.org/10.1038/nature05459.

(9) Bieling, P.; Li, T.-D.; Weichsel, J.; McGorty, R.; Jreij, P.; Huang, B.; Fletcher, D. A.; Mullins, R. D. Force Feedback Controls Motor Activity and Mechanical Properties of Self-Assembling Branched Actin Networks. *Cell* **2016**, *164* (1–2), 115–127. https://doi.org/10.1016/j.cell.2015.11.057.

(10) Bauër, P.; Tavacoli, J.; Pujol, T.; Planade, J.; Heuvingh, J.; du Roure, O. A New Method to Measure Mechanics and Dynamic Assembly of Branched Actin Networks. *Sci. Rep.* **2017**, *7* (1), 15688. https://doi.org/10.1038/s41598-017-15638-5.

(11) Weinberg, J.; Drubin, D. G. Clathrin-Mediated Endocytosis in Budding Yeast. *Trends Cell Biol.* **2012**, *22* (1), 1–13. https://doi.org/10.1016/j.tcb.2011.09.001.

(12) Kaksonen, M.; Roux, A. Mechanisms of Clathrin-Mediated Endocytosis. *Nat. Rev. Mol. Cell Biol.* **2018**, *19* (5), 313–326. https://doi.org/10.1038/nrm.2017.132.

(13) Lu, R.; Drubin, D. G.; Sun, Y. Clathrin-Mediated Endocytosis in Budding Yeast at a Glance. *J. Cell Sci.* **2016**, *129* (8), 1531–1536. https://doi.org/10.1242/jcs.182303.

(14) Stachowiak, J. C.; Brodsky, F. M.; Miller, E. A. A Cost–Benefit Analysis of the Physical Mechanisms of Membrane Curvature. *Nat. Cell Biol.* **2013**, *15* (9), 1019–1027. https://doi.org/10.1038/ncb2832.

(15) Boulant, S.; Kural, C.; Zeeh, J.-C.; Ubelmann, F.; Kirchhausen, T. Actin Dynamics Counteract Membrane Tension during Clathrin-Mediated Endocytosis. *Nat. Cell Biol.* **2011**, *13* (9), 1124–1131. https://doi.org/10.1038/ncb2307.

(16) Aghamohammadzadeh, S.; Ayscough, K. R. Differential Requirements for Actin during Yeast and Mammalian Endocytosis. *Nat. Cell Biol.* **2009**, *11* (8), 1039–1042. https://doi.org/10.1038/ncb1918.

(17) Basu, R.; Munteanu, E. L.; Chang, F. Role of Turgor Pressure in Endocytosis in Fission Yeast. *Mol. Biol. Cell* **2014**, *25* (5), 679–687. https://doi.org/10.1091/mbc.e13-10-0618.

(18) Carlsson, A. E.; Bayly, P. V. Force Generation by Endocytic Actin Patches in Budding Yeast. *Biophys. J.* **2014**, *106* (8), 1596–1606. https://doi.org/10.1016/j.bpj.2014.02.035.

(19) Klis, F. M. Review: Cell Wall Assembly in Yeast. *Yeast* **1994**, *10* (7), 851–869. https://doi.org/10.1002/yea.320100702.

(20) Minc, N.; Boudaoud, A.; Chang, F. Mechanical Forces of Fission Yeast Growth. *Curr. Biol.* **2009**, *19* (13), 1096–1101. https://doi.org/10.1016/j.cub.2009.05.031.

(21) Schaber, J.; Adrover, M. À.; Eriksson, E.; Pelet, S.; Petelenz-Kurdziel, E.; Klein, D.; Posas, F.; Goksör, M.; Peter, M.; Hohmann, S.; Klipp, E. Biophysical Properties of Saccharomyces Cerevisiae and Their Relationship with HOG Pathway Activation. *Eur. Biophys. J.* **2010**, *39* (11), 1547–1556. https://doi.org/10.1007/s00249-010-0612-0.

(22) Goldenbogen, B.; Giese, W.; Hemmen, M.; Uhlendorf, J.; Herrmann, A.; Klipp, E. Dynamics of Cell Wall Elasticity Pattern Shapes the Cell during Yeast Mating Morphogenesis. *Open Biol.* **2016**, *6* (9), 160136. https://doi.org/10.1098/rsob.160136.

(23) Dmitrieff, S.; Nédélec, F. Amplification of Actin Polymerization Forces. *J. Cell Biol.* **2016**, *212* (7), 763–766. https://doi.org/10.1083/jcb.201512019.

(24) Mund, M.; van der Beek, J. A.; Deschamps, J.; Dmitrieff, S.; Hoess, P.; Monster, J. L.; Picco, A.; Nédélec, F.; Kaksonen, M.; Ries, J. Systematic Nanoscale Analysis of Endocytosis Links Efficient Vesicle Formation to Patterned Actin Nucleation. *Cell* **2018**, *174* (4), 884-896.e17. https://doi.org/10.1016/j.cell.2018.06.032.

(25) Akamatsu, M.; Vasan, R.; Serwas, D.; Ferrin, M. A.; Rangamani, P.; Drubin, D. G. Principles of Self-Organization and Load Adaptation by the Actin Cytoskeleton during Clathrin-Mediated Endocytosis. *eLife* **2020**, *9*, e49840. https://doi.org/10.7554/eLife.49840.

(26) Sirotkin, V.; Berro, J.; Macmillan, K.; Zhao, L.; Pollard, T. D. Quantitative Analysis of the Mechanism of Endocytic Actin Patch Assembly and Disassembly in Fission Yeast. *Mol. Biol. Cell* **2010**, *21* (16), 2894–2904. https://doi.org/10.1091/mbc.e10-02-0157.

(27) Berro, J.; Sirotkin, V.; Pollard, T. D. Mathematical Modeling of Endocytic Actin Patch Kinetics in Fission Yeast: Disassembly Requires Release of Actin Filament Fragments. *Mol. Biol. Cell* **2010**, *21* (16), 2905–2915. https://doi.org/10.1091/mbc.e10-06-0494.

(28) Wang, X.; Galletta, B. J.; Cooper, J. A.; Carlsson, A. E. Actin-Regulator Feedback Interactions during Endocytosis. *Biophys. J.* **2016**, *110* (6), 1430–1443. https://doi.org/10.1016/j.bpj.2016.02.018.

(29) Lacy, M. M.; Ma, R.; Ravindra, N. G.; Berro, J. Molecular Mechanisms of Force Production in Clathrin-Mediated Endocytosis. *FEBS Lett.* **2018**, *592* (21), 3586–3605. https://doi.org/10.1002/1873-3468.13192.

(30) Dmitrieff, S.; Nédélec, F. Membrane Mechanics of Endocytosis in Cells with Turgor. *PLOS Comput. Biol.* **2015**, *11* (10), e1004538. https://doi.org/10.1371/journal.pcbi.1004538.

(31) Carlsson, A. E. Membrane Bending by Actin Polymerization. *Curr. Opin. Cell Biol.* **2018**, *50*, 1–7. https://doi.org/10.1016/j.ceb.2017.11.007.

(32) Manenschijn, H. E.; Picco, A.; Mund, M.; Rivier-Cordey, A.-S.; Ries, J.; Kaksonen, M. Type-I Myosins Promote Actin Polymerization to Drive Membrane Bending in Endocytosis. *eLife* **2019**, *8*, e44215. https://doi.org/10.7554/eLife.44215.

(33) Ma, R.; Berro, J. Structural Organization and Energy Storage in Crosslinked Actin Assemblies. *PLOS Comput. Biol.* **2018**, *14* (5), e1006150. https://doi.org/10.1371/journal.pcbi.1006150.

(34) Nickaeen, M.; Berro, J.; Pollard, T. D.; Slepchenko, B. M. Actin Assembly Produces Sufficient Forces for Endocytosis in Yeast. *Mol. Biol. Cell* **2019**, *30* (16), 2014–2024. https://doi.org/10.1091/mbc.E19-01-0059.

(35) Kaksonen, M.; Toret, C. P.; Drubin, D. G. A Modular Design for the Clathrin- and Actin-Mediated Endocytosis Machinery. *Cell* **2005**, *123* (2), 305–320. https://doi.org/10.1016/j.cell.2005.09.024.

(36) Picco, A.; Kukulski, W.; Manenschijn, H. E.; Specht, T.; Briggs, J. A. G.; Kaksonen, M. The Contributions of the Actin Machinery to Endocytic Membrane Bending and Vesicle Formation. *Mol. Biol. Cell* **2018**, *29* (11), 1346–1358. https://doi.org/10.1091/mbc.E17-11-0688.

(37) Planade, J.; Belbahri, R.; Boiero Sanders, M.; Guillotin, A.; du Roure, O.; Michelot, A.; Heuvingh, J. Mechanical Stiffness of Reconstituted Actin Patches Correlates Tightly with Endocytosis Efficiency. *PLOS Biol.* **2019**, *17* (10), e3000500. https://doi.org/10.1371/journal.pbio.3000500.

(38) Skau, C. T.; Courson, D. S.; Bestul, A. J.; Winkelman, J. D.; Rock, R. S.; Sirotkin, V.; Kovar, D. R. Actin Filament Bundling by Fimbrin Is Important for Endocytosis, Cytokinesis, and Polarization in Fission Yeast. *J. Biol. Chem.* **2011**, *286* (30), 26964–26977. https://doi.org/10.1074/jbc.M111.239004.

(39) Lieleg, O.; Claessens, M. M. A. E.; Bausch, A. R. Structure and Dynamics of Cross-Linked Actin Networks. *Soft Matter* **2010**, *6* (2), 218–225. https://doi.org/10.1039/B912163N.

(40) Michelot, A.; Costanzo, M.; Sarkeshik, A.; Boone, C.; Yates, J. R.; Drubin, D. G. Reconstitution and Protein Composition Analysis of Endocytic Actin Patches. *Curr. Biol.* **2010**, *20* (21), 1890–1899. https://doi.org/10.1016/j.cub.2010.10.016.

(41) Pujol, T.; du Roure, O.; Fermigier, M.; Heuvingh, J. Impact of Branching on the Elasticity of Actin Networks. *Proc. Natl. Acad. Sci.* **2012**, *109* (26), 10364–10369. https://doi.org/10.1073/pnas.1121238109.

(42) Tinevez, J.-Y.; Perry, N.; Schindelin, J.; Hoopes, G. M.; Reynolds, G. D.; Laplantine, E.; Bednarek, S. Y.; Shorte, S. L.; Eliceiri, K. W. TrackMate: An Open and Extensible Platform for Single-Particle Tracking. *Methods* **2017**, *115*, 80–90. https://doi.org/10.1016/j.ymeth.2016.09.016.

(43) Kukulski, W.; Schorb, M.; Kaksonen, M.; Briggs, J. A. G. Plasma Membrane Reshaping during Endocytosis Is Revealed by Time-Resolved Electron Tomography. *Cell* **2012**, *150* (3), 508–520. https://doi.org/10.1016/j.cell.2012.05.046.

(44) Michelot, A.; Drubin, D. G. Chapter Twenty-One - Dissecting Principles Governing Actin Assembly Using Yeast Extracts. In *Reconstituting the Cytoskeleton*; Vale, R. D., Ed.; Methods in Enzymology; Academic Press, 2014; Vol. 540, pp 381–397. https://doi.org/10.1016/B978-0-12-397924-7.00021-2.

(45) Longtine, M. I.; Demarini, S.; Wach, B.; Philippsen, P. Additional Modules for Versatile and Economical PCR-Based Gene Deletion and Modification in Saccharomyces Cerevisiae. **1998**, 9.
(46) Antkowiak, A.; Guillotin, A.; Boiero Sanders, M.; Colombo, J.; Vincentelli, R.; Michelot, A. Sizes of Actin Networks Sharing a Common Environment Are Determined by the Relative Rates of Assembly. *PLOS Biol.* **2019**, *17* (6), e3000317. https://doi.org/10.1371/journal.pbio.3000317.
(47) Tavacoli, J. W.; Bauër, P.; Fermigier, M.; Bartolo, D.; Heuvingh, J.; du Roure, O. The Fabrication and Directed Self-Assembly of Micron-Sized Superparamagnetic Non-Spherical Particles. *Soft Matter* **2013**, *9* (38), 9103. https://doi.org/10.1039/c3sm51589c.
(48) Bausch, A. R.; Ziemann, F.; Boulbitch, A. A.; Jacobson, K.; Sackmann, E. Local Measurements of Viscoelastic Parameters of Adherent Cell Surfaces by Magnetic Bead Microrheometry. *Biophys. J.* **1998**, *75* (4), 2038–2049. https://doi.org/10.1016/S0006-3495(98)77646-5.
(49) Desprat, N.; Richert, A.; Simeon, J.; Asnacios, A. Creep Function of a Single Living Cell. *Biophys. J.* **2005**, *88* (3), 2224–2233. https://doi.org/10.1529/biophysj.104.050278.
(50) Broedersz, C. P.; Mao, X.; Lubensky, T. C.; MacKintosh, F. C. Criticality and Isostaticity in Fibre Networks. *Nat. Phys.* **2011**, *7* (12), 983–988. https://doi.org/10.1038/nphys2127.
(51) Noireaux, V.; Golsteyn, R. M.; Friederich, E.; Prost, J.; Antony, C.; Louvard, D.; Sykes, C. Growing an Actin Gel on Spherical Surfaces. *Biophys. J.* **2000**, *78* (3), 1643–1654. https://doi.org/10.1016/S0006-3495(00)76716-6.
(52) Dafalias, Y. F.; Pitouras, Z. Stress Field in Actin Gel Growing on Spherical Substrate. *Biomech. Model. Mechanobiol.* **2009**, *8* (1), 9–24. https://doi.org/10.1007/s10237-007-0113-y.
(53) Mueller, J.; Szep, G.; Nemethova, M.; de Vries, I.; Lieber, A. D.; Winkler, C.; Kruse, K.; Small, J. V.; Schmeiser, C.; Keren, K.; Hauschild, R.; Sixt, M. Load Adaptation of Lamellipodial Actin Networks. *Cell* **2017**, *171* (1), 188-200.e16. https://doi.org/10.1016/j.cell.2017.07.051.
(54) Okreglak, V.; Drubin, D. G. Cofilin Recruitment and Function during Actin-Mediated Endocytosis Dictated by Actin Nucleotide State. *J. Cell Biol.* **2007**, *178* (7), 1251–1264. https://doi.org/10.1083/jcb.200703092.
(55) Okreglak, V.; Drubin, D. G. Loss of Aip1 Reveals a Role in Maintaining the Actin Monomer Pool and an in Vivo Oligomer Assembly Pathway. *J. Cell Biol.* **2010**, *188* (6), 769–777. https://doi.org/10.1083/jcb.200909176.
(56) Lin, M.-C.; Galletta, B. J.; Sept, D.; Cooper, J. A. Overlapping and Distinct Functions for Cofilin, Coronin and Aip1 in Actin Dynamics in Vivo. *J. Cell Sci.* **2010**, *123* (8), 1329–1342. https://doi.org/10.1242/jcs.065698.

Supplementary figure

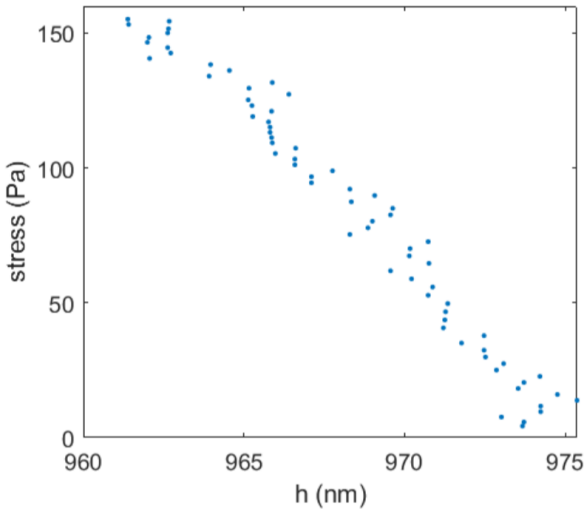

	K50 (kPa)
Exp1	8.4
Exp2	7.3
Exp3	7.7
Exp4	9.7
Exp5	5.4

Left: Deformation as a function of applied stress of a reconstituted actin patch (from WT extract) which has grown under an applied stress of ~80 Pa. Right: Table of tangent modulus at 50 Pa of the patch on the left as well as four replicates on different patches grown under 80 Pa stress.